

A Parameter-efficient Convolutional Approach for Weed Detection in Multispectral Aerial Imagery

Leo Thomas Ramos^{1,2} (lramos@cvc.uab.cat) Angel D. Sappa^{1,2,3} (sappa@ieee.org)
¹Computer Vision Center ²Universitat Autònoma de Barcelona ³ESPOL Polytechnic University

Abstract

We introduce *FCBNet*, an efficient model designed for weed segmentation. The architecture is based on a fully frozen ConvNeXt backbone, the proposed Feature Correction Block (FCB), which leverages efficient convolutions for feature refinement, and a lightweight decoder. *FCBNet* is evaluated on the WeedBananaCOD and WeedMap datasets under both RGB and multispectral modalities, showing that *FCBNet* outperforms models such as U-Net, DeepLabV3+, SK-U-Net, SegFormer, and WeedSense in terms of mIoU, exceeding 85%, while also achieving superior computational efficiency, requiring only 0.06 to 0.2 hours for training. Furthermore, the frozen backbone strategy reduces the number of trainable parameters by more than 90%, significantly lowering memory requirements. Code available at: [hidden_for_review](#)

1. Introduction

Weeds are unwanted plant species that grow alongside crops and compete for essential resources such as nutrients, water, sunlight, and space [22]. As a result, weeds are recognized as one of the primary factors contributing to yield reduction across a wide range of cropping systems [5, 22], reducing overall agricultural efficiency. At a broader scale, these effects result in substantial economic losses and negatively impact productivity [28], profitability [23], and the stability of supply chains [21].

Traditional detection relies on manual field inspection [6], where farmers visually identify weed presence across cultivated areas. However, agricultural fields often extend over large areas, making this process labor-intensive [21], time-consuming [19], and difficult to perform consistently [23]. This reduces the frequency and spatial coverage of inspections, increasing the risk of delayed or incomplete detection [12]. Accordingly, this lack of precise monitoring affects subsequent management decisions [1, 34], since effective treatment depends on accurate knowledge of weed location and distribution within the field [1].

To address these limitations, Deep Learning (DL)-based

approaches have gained significant attention [21, 42], particularly semantic segmentation methods [15, 21]. These models are trained on large datasets and learn discriminative patterns from visual features such as colour, texture, and shape [24]. Consequently, they enable automatic identification and precise delineation of weeds at the pixel level [18], providing detailed information about their presence and spatial distribution. This facilitates large-scale analysis and supports more accurate and consistent monitoring compared to manual inspection [32].

Nonetheless, DL models face practical limitations. Achieving high accuracy commonly requires complex architectures with millions of trainable parameters [2], resulting in high computational and memory requirements during training [27, 28]. Also, deployment conditions impose strict constraints, since the models are often required to operate in open and remote agricultural environments [28] without access to high-performance computing infrastructure [14], and are typically integrated into platforms such as UAVs and drones with limited capacity [35]. Furthermore, multispectral/multimodal imagery is frequently employed in this domain [7, 31, 36, 37], which increases the computational requirements and data processing complexity.

Several strategies exist to obtain efficient models, but they have specific trade-offs. Model distillation transfers the knowledge from a large model to a smaller one with reduced latency [8], but it often requires a pre-trained high-capacity teacher and an distillation stage that introduces non-negligible overhead [4, 39]. Transfer learning adapts representations learned from a source domain to a target domain [20, 45], yet segmentation often requires fine-tuning a significant portion of the model [13, 46], since features for classification do not preserve the spatial and boundary information required for mask reconstruction [43, 44].

Likewise, model freezing reduces memory usage and the number of trainable parameters [40], but introduces a mismatch between fixed feature representations and the reconstruction requirements of the decoder. This often requires introducing heavy adaptation blocks to achieve competitive accuracy [11], which undermines the intended efficiency of using a frozen backbone. Therefore, developing accurate

yet efficient models remains an open research challenge.

Based on the above, we propose a DL approach for weed detection, aiming to achieve high accuracy while maintaining training efficiency and low latency. To this end, we adopt the model freezing paradigm, as it is one of the most effective methods for reducing the number of trainable parameters and computational cost. Hence, we employ a fully-frozen ConvNeXt [17] backbone integrated with a Feature Pyramid Network [16] (FPN)-based decoder for segmentation. To handle the existing mismatch, we introduce Feature Correction Blocks (FCBs), which are inserted after each ConvNeXt extraction stage to refine the features passed to the decoder. These blocks are composed of pointwise and depthwise convolutions to preserve efficiency, along with group normalization to stabilize training independently of batch size.

The proposed model is evaluated on two aerial image datasets for weed detection, covering both RGB and multispectral scenarios. The results demonstrate superior performance compared to established and state-of-the-art models. Furthermore, the use of ConvNeXt enables leveraging its stage-based design to incorporate the same number of FCBs across all its variants, regardless of their complexity. Consequently, a reduction of more than 90% in the number of trainable parameters is achieved, while maintaining superior performance and low latency. The contributions of this work are as follows:

- We propose FCBNet, an efficient model for weed detection.
- We introduce the Feature Correction Block, which refines feature representations from a frozen backbone with minimal computational cost.
- We show that the proposed freezing strategy reduces the number of trainable parameters by more than 90%.
- We show that FCBNet achieves low latency and fast training without compromising segmentation performance.

2. Related work

Numerous DL approaches for weed detection have been developed in recent years. Increasing attention has been given to model performance, although not without important trade-offs. For instance, [9] proposes a semi supervised adversarial framework based on a U-Net with a ResNet50 backbone and a convolutional discriminator, enabling the use of unlabelled UAV RGB images through pseudo labelling. The method reduces annotation requirements, but the training process requires additional iterations.

The work by [35] uses a densely connected feed forward Deep Neural Network (DNN) combining handcrafted color and texture descriptors from UAV RGB images to improve weed discrimination. While it achieves high performance, the DNN training involves strenuous and prolonged processing. Similarly, [37] proposes CGS-YOLO for multi-

spectral weed detection that incorporates CARAFE upsampling, attention mechanisms, and an additional small target detection layer to improve small instance identification. While this improves discrimination capability, parameter count and complexity increase due to the additional head and feature fusion operations.

In the same way, [31] proposes a ResNet-50-backed U-Net combined with a fully connected Conditional Random Field (CRF) for boundary refinement. The method introduces a composite 3-channel input derived from spectral transformations to reduce computational cost. However, the CRF refinement increases post processing complexity. Likewise, [10] proposes a multi-class detection approach using U-Net and hybrid variants with pre-trained encoders (VGG19, MobileNetV2, and InceptionResNetV2). While deeper backbones achieve higher performance, they substantially increase model size and computational cost.

Other methods focus on improving efficiency to enable real-world deployment, although this often introduces performance limitations. The work by [27], for example, proposes a weed detection system based on superpixel segmentation and lightweight CNN classifiers, targeting deployment on embedded devices such as Raspberry Pi. It explores custom shallow architectures, pruning, and quantization to reduce model size and latency. However, aggressive quantization introduced accuracy degradation.

SC-Net [15] uses a U-Net based model with multi-scale convolutional blocks and attention based feature fusion to improve weed localization while reducing computational cost. Strip convolutions enlarges the receptive field with lower complexity, enabling efficient feature extraction. However, this degrades shallow feature representation and reduce performance in small regions, while the model size remains non-trivial. Similarly, [47] proposes a U-Net network with a reduced VGG backbone to improve computational efficiency. The model is pre-trained using synthetic images and later fine-tuned on real data, enabling accurate, low-latency segmentation. However, this limits feature extraction, reducing suitability for complex scenarios.

As seen, progress is driven either by strategies and components that push identification performance, or by efficiency oriented designs intended to reduce deployment cost. However, accuracy gains are often accompanied by increased training time or parameter count that raise resource demands. Conversely, approaches that prioritize compactness can reduce latency and memory footprint, but usually exhibit performance degradation under challenging conditions, highlighting the persistent trade-off between computational efficiency and robust weed identification.

3. Model design

The proposed model follows an encoder-decoder design, as shown in Fig. 1. It uses a fully frozen ConvNeXt backbone

that produces four multi-scale feature maps, and inserts FCBs after each extraction stage to refine and correct the features. The corrected stage features are then integrated by a lightweight FPN-based decoder operating over the same four levels, which reconstructs a high-resolution representation. This representation is subsequently processed by a compact segmentation head to generate the final segmentation mask. We refer to this model as FCBNet. Below, we present each component of the architecture in detail.

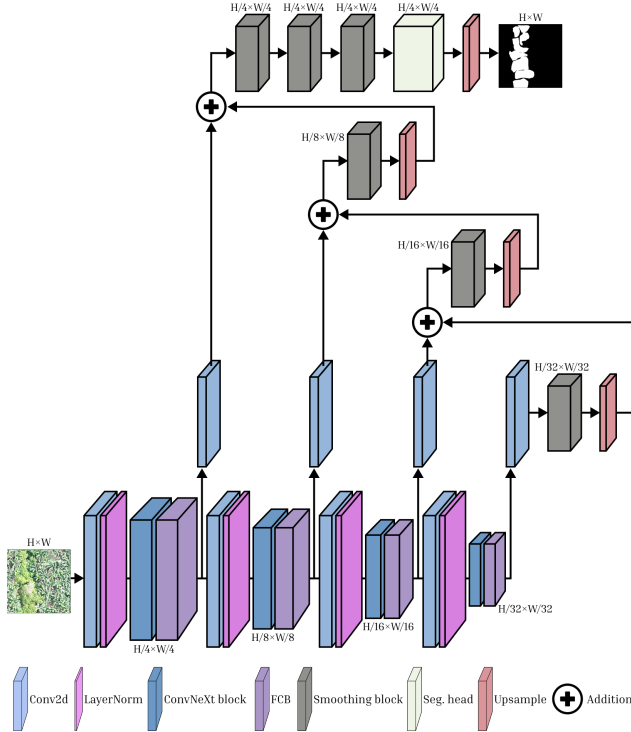


Figure 1. Overview of FCBNet proposed in this work.

3.1. Encoder

FCBNet’s encoder is based on ConvNeXt as its underlying backbone. ConvNeXt is a Convolutional Neural Network (CNN) that builds upon ResNet50 by introducing a stage-wise design, layer normalization, GELU activations, and larger convolutional kernels (7×7). This enables effective hierarchical representation learning with controlled computational cost. A ConvNeXt block can be seen in Fig. 2.

The selection of ConvNeXt in this work is motivated by its architectural design. ConvNeXt was developed with the goal of achieving performance comparable to Transformers, which currently represent the state-of-the-art in computer vision. However, Transformers exhibit quadratic complexity and require large amounts of data and training time to achieve strong performance. In response, ConvNeXt modernizes conventional CNNs through a Transformer-inspired design while preserving the efficiency advantages of CNNs.

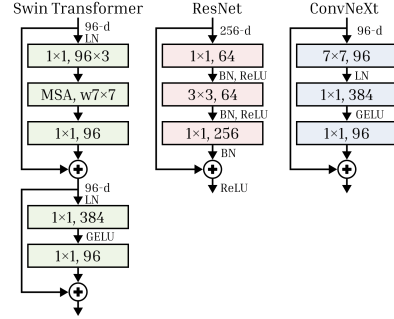


Figure 2. Comparison between ResNet, Swin Transformer, and ConvNeXt blocks.

Table 1. ConvNeXt variants and their details.

Model	Channels (per stage)	Depths (per stage)	Params (M)
ConvNeXt-tiny	[96, 192, 384, 768]	[3, 3, 9, 3]	28
ConvNeXt-small	[96, 192, 384, 768]	[3, 3, 27, 3]	50
ConvNeXt-base	[128, 256, 512, 1024]	[3, 3, 27, 3]	89
ConvNeXt-large	[192, 384, 768, 1536]	[3, 3, 27, 3]	198

Based on the above, ConvNeXt is selected as the feature extractor of FCBNet, as it provides an effective balance between the representation capability of Transformers and the computational efficiency of CNNs, which is consistent with the objective of our approach. ConvNeXt is available in four variants, as shown in Table 1. In this work, ConvNeXt-base (Fig. 3) is used as the default configuration of FCBNet.

Feature Correction Block As mentioned, ConvNeXt is an efficient and high-performance architecture well-suited for feature extraction. However, it has a non-trivial number of parameters, particularly in its larger variants, which can limit its suitability for deployment in resource-constrained environments. Furthermore, a segmentation model also requires the inclusion of a decoder and a segmentation head, which further increases the overall model complexity.

To maximize the efficient use of ConvNeXt, we employ it in a fully frozen configuration. This results in a substantial reduction in the number of trainable parameters, but also causes the feature representations to remain optimized for the original task and unable to be refined during training for the new domain. This, in turn, causes the decoder to operate

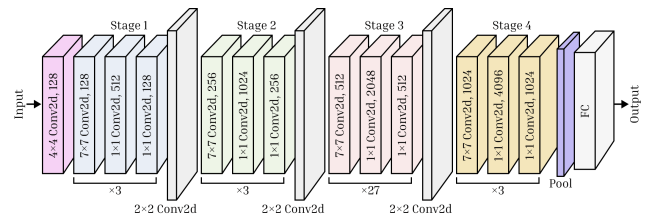


Figure 3. ConvNeXt-base architecture. Adapted from: [26]

on suboptimal feature representations, limiting its ability to accurately reconstruct the segmentation mask.

To address the mismatch between the fixed encoder features and the decoder requirements, we introduce the Feature Correction Block (FCB). FCB is a lightweight residual module designed to operate on convolutional feature maps. Its objective is to refine and adapt the features extracted by the backbone, enabling more effective integration by the decoder while preserving computational efficiency.

A FCB comprises seven layers in a bottleneck-like structure: a Pointwise convolution (PWConv), followed by Group Normalization (GroupNorm) with GELU activation, a Depthwise convolution (DWConv), a second GroupNorm + GELU, and a final PWConv. In addition, each FCB incorporates a residual connection that links the input and output of each block, that allows it to introduce corrective modifications while preserving the original feature information.

PWConv and DWConv are a design choice for computational efficiency. PWConv (1×1) enables channel-wise feature projection with minimal overhead, while DWConv captures spatial context at significantly lower cost than standard convolutions. Likewise, GroupNorm is used to stabilize optimization without relying on large batch sizes, which is particularly useful under resource constrained training settings.

Mathematically, FCB implements a transformation $f(\cdot)$ over the input tensor $x \in \mathbb{R}^{B \times C \times H \times W}$, as in Eq. 1:

$$y = x + \alpha f(x), \quad (1)$$

where $f(\cdot)$ operates in a lower dimensional embedded space, applies spatial processing, and produces a correction term that is added to the input through a residual connection scaled by the learnable parameter $\alpha \in \mathbb{R}$.

The transformation $f(x)$ follows a bottleneck structure composed of efficient convolutional operations. First, the input tensor with C channels is projected into an intermediate space of dimensionality C' defined in Eq. 2:

$$C' = \max \left(C_{\min}, \left\lfloor \frac{C}{r} \right\rfloor \right), \quad (2)$$

where r corresponds to the bottleneck ratio controlling the channel reduction, and C_{\min} is a lower bound imposed to ensure sufficient representational capacity. This projection is implemented using a bias free 1×1 convolution, followed by GroupNorm and a GELU activation, as in Eq. 3:

$$z_1 = \phi \left(\text{GroupNorm}_1 \left(\text{Conv}_{1 \times 1}^{C \rightarrow C'}(x) \right) \right), \quad (3)$$

where, $\phi(\cdot)$ denotes the GELU activation function. Next, a DWConv with kernel size $k \times k$ is applied to model spatial context efficiently, again followed by GroupNorm and GELU, as shown in Eq. 4:

$$z_2 = \phi \left(\text{GroupNorm}_2 \left(\text{DWConv}_{k \times k}(z_1) \right) \right). \quad (4)$$

Finally, the representation is projected back to the original channel dimensionality using another 1×1 convolution, as in Eq. 5:

$$f(x) = \text{Conv}_{1 \times 1}^{C' \rightarrow C}(z_2). \quad (5)$$

In our implementation, the number of GroupNorm groups is dynamically selected to exactly divide the number of channels C' , preventing invalid configurations when C' is small or not divisible by the preferred number of groups. The entire refining process is achieved using lightweight operations, avoiding the heavy parameter and computational overhead of alternative mechanisms like attention modules.

Within the frozen ConvNeXt encoder, one FCB is inserted immediately after each feature extraction stage, allowing progressive correction of the multi-scale representations. Since all ConvNeXt variants share the same four-stage hierarchical structure, the number of FCBs remains constant regardless of the backbone complexity.

3.2. Decoder and head

To fuse the features extracted by the encoder, we employ a lightweight FPN-based decoder. It integrates four multi-scale feature maps into a single, high-resolution representation optimized for segmentation. Additionally, the design is streamlined to maintain computational efficiency.

Specifically, it includes four 1×1 convolutions that project the feature maps from each encoder stage into a shared channel dimensionality. These are followed by four smoothing blocks, each consisting of a 3×3 convolution, BatchNorm, and GELU activation. These blocks are used during the top-down fusion process, where lower resolution features are upsampled using bilinear interpolation and combined with higher resolution features through element wise summation. Two additional smoothing blocks form a refinement stage applied at the highest resolution to further consolidate the decoded features before prediction.

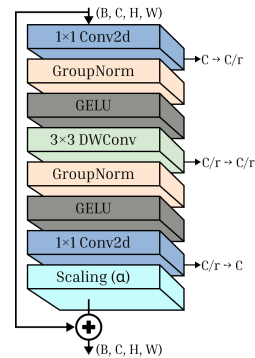


Figure 4. Structure of the Feature Correction Block.

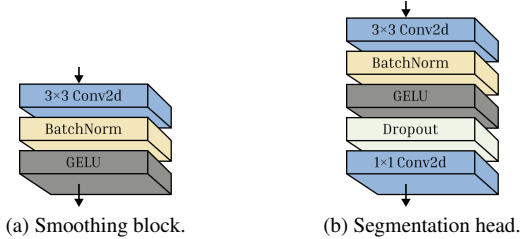


Figure 5. Smoothing block and head used in FCBNet decoder.

Finally, a compact segmentation head converts the decoder features into class predictions. The head uses a 3×3 convolution followed by BatchNorm and GELU, applies dropout for regularization, and then uses a final 1×1 convolution to map features to the desired number of output channels. The resulting logits are upsampled to the original input resolution using bilinear interpolation, producing the final full-resolution segmentation mask.

4. Experiments

4.1. Datasets and preprocessing

To evaluate the proposed model, two aerial imagery datasets, WeedBananaCOD [38] and WeedMap [30], for weed detection are selected.

WeedBananaCOD [38] is an aerial dataset for camouflaged weed detection. The images were acquired over an approximately 4.3 hectare banana field located in the coastal region of Ecuador. The site is characterized by dense and homogeneous vegetation, creating challenging conditions where weeds are often visually camouflaged within the surrounding crop. Images were captured using a MicaSense RedEdge-M camera mounted on a DJI Mavic 2 Pro UAV. The dataset is multispectral, including RGB and near infrared (NIR) bands, and comprises a tile of size 5571×5855 pixels. The images were divided into 512×512 patches using the official preprocessing code provided by the authors.

WeedMap [30] is one of the best-known datasets for weed detection. It was acquired in sugar beet fields located in Switzerland and Germany. It consists of two subsets: one captured with a RedEdge-M camera mounted on a DJI Inspire 2 UAV, providing five spectral bands (RGB, NIR, and red edge (RE)), and another by a Sequoia camera mounted on a DJI Mavic Pro UAV with RGB-NIR configuration. In this work, the RedEdge-M subset¹ (5964 images of 480×360 pixels) was selected, as it contains a larger number of images with weed presence, while the Sequoia subset includes a higher proportion of other vegetation classes.

¹Note that WeedMap contains multiple semantic classes; for this study, all non-weed classes were merged into the background to enable binary segmentation.

4.2. Experimental setup

Training is conducted in a Python environment using cross entropy loss and the AdamW optimizer. The learning rate is set to $1e-3$ and scheduled using a OneCycle policy. Models were trained for 100 epochs with a batch size of 64 on an NVIDIA A100 GPU with 40 GB of memory. For comparison, several semantic segmentation models were trained under the same configuration, including established architectures and weed specific methods such as U-Net [29], DeepLabV3+ [3], SegFormer [41], SK-UNet [25], and WeedSense [33].

Performance is evaluated using the main semantic segmentation metrics, including intersection over union (IoU) for weed and background classes, and mean IoU (mIoU). Computational efficiency is assessed by measuring inference time (average latency per image), training time, total number of parameters, number of trainable parameters, and GFLOPs. The experiments were conducted using both RGB and full spectral configurations. To support additional channels, the first layer of each model is expanded accordingly.

4.3. Results and discussion

Table 2 evaluates the impact of the α parameter on model performance. Results show a modest but consistent improvement as α increases, with the best performance achieved at $\alpha = 0.07$ across both RGB and multispectral configurations. This indicates that stronger feature correction improves representation quality. Beyond 0.07, performance degrades, suggesting that excessive correction disrupts feature stability rather than enhancing discrimination. Also, α has no effect on efficiency, as parameter count, GFLOPs, and latency remain constant.

Table 2. Ablation of the FCB α parameter for feature refinement.

Alpha	Dataset	Modality	IoU _{we} †	IoU _{bg} †	mIoU †	Inference time (s)	Training time (h)	Total params. (M)	Trainable params. (M)	GFLOPs
0.01	WeedBananaCOD	RGB	0.990	0.730	0.860	0.0236	0.101	91.277	2.685	15.156
		RGB-NIR	0.991	0.754	0.873	0.0237	0.106	91.279	2.685	15.190
	WeedMap	RGB	0.985	0.531	0.758	0.0141	0.129	91.277	2.685	10.657
		RGB-NIR	0.986	0.531	0.759	0.0144	0.137	91.279	2.685	10.680
		RGB-NIR-RE	0.986	0.536	0.761	0.0147	0.144	91.281	2.685	10.704
	0.03	WeedBananaCOD	RGB	0.990	0.732	0.861	0.0253	0.103	91.277	2.685
RGB-NIR			0.991	0.747	0.869	0.0279	0.108	91.279	2.685	15.190
WeedMap		RGB	0.983	0.529	0.756	0.0173	0.132	91.277	2.685	10.657
		RGB-NIR	0.986	0.531	0.759	0.0175	0.140	91.279	2.685	10.680
		RGB-NIR-RE	0.986	0.535	0.761	0.0179	0.146	91.281	2.685	10.704
0.05		WeedBananaCOD	RGB	0.990	0.722	0.856	0.0254	0.102	91.277	2.685
	RGB-NIR		0.992	0.760	0.876	0.0281	0.109	91.279	2.685	15.190
	WeedMap	RGB	0.985	0.527	0.756	0.0158	0.130	91.277	2.685	10.657
		RGB-NIR	0.985	0.530	0.758	0.0164	0.138	91.279	2.685	10.680
		RGB-NIR-RE	0.985	0.532	0.759	0.0169	0.145	91.281	2.685	10.704
	0.07	WeedBananaCOD	RGB	0.991	0.733	0.862	0.0227	0.099	91.277	2.685
RGB-NIR			0.991	0.762	0.877	0.0298	0.105	91.279	2.685	15.190
WeedMap		RGB	0.985	0.534	0.760	0.0141	0.128	91.277	2.685	10.657
		RGB-NIR	0.986	0.545	0.766	0.0145	0.134	91.279	2.685	10.680
		RGB-NIR-RE	0.987	0.547	0.767	0.0147	0.142	91.281	2.685	10.704
0.09		WeedBananaCOD	RGB	0.990	0.713	0.851	0.0215	0.104	91.277	2.685
	RGB-NIR		0.991	0.749	0.870	0.0240	0.105	91.279	2.685	15.190
	WeedMap	RGB	0.984	0.532	0.758	0.0169	0.130	91.277	2.685	10.657
		RGB-NIR	0.985	0.531	0.758	0.0177	0.143	91.279	2.685	10.680
		RGB-NIR-RE	0.986	0.537	0.762	0.0172	0.144	91.281	2.685	10.704

The ablation of the FCB bottleneck ratio is shown in Table 3. The results indicate that a configuration of 2 represents the optimal balance point. Due to the inverse na-

ture of this parameter in the FCB block, increasing this ratio reduces model complexity and accelerates computation, as higher values decrease the number of internal channels. However, ratios above 2 lead to performance degradation. The excessive reduction in internal dimensionality limits the model’s representational capacity, preventing the block from capturing the fine details required for segmentation and resulting in a gradual loss of accuracy.

Table 3. Ablation of the of the FCB bottleneck ratio.

Bottleneck ratio	Dataset	Modality	IoU _{BC} ↑	IoU _w ↑	mIoU ↑	Inference time (s)	Training time (h)	Total params. (M)	Trainable params. (M)	GFLOPs
1	WeedBananaCOD	RGB	0.991	0.739	0.865	0.0248	0.107	92.682	4.090	16.260
		RGB-NIR	0.991	0.752	0.872	0.0306	0.112	92.684	4.090	16.293
	WeedMap	RGB	0.985	0.517	0.751	0.0167	0.135	92.682	4.090	11.432
		RGB-NIR	0.984	0.520	0.752	0.0169	0.139	92.684	4.090	11.456
		RGB-NIR-RE	0.985	0.537	0.761	0.0171	0.148	92.686	4.090	11.480
	2	WeedBananaCOD	RGB	0.991	0.733	0.862	0.0227	0.099	91.277	2.685
RGB-NIR			0.991	0.762	0.877	0.0298	0.105	91.279	2.685	15.190
WeedMap		RGB	0.985	0.534	0.760	0.0141	0.128	91.277	2.685	10.657
		RGB-NIR	0.986	0.545	0.766	0.0145	0.134	91.279	2.685	10.680
		RGB-NIR-RE	0.987	0.547	0.767	0.0147	0.142	91.281	2.685	10.704
3		WeedBananaCOD	RGB	0.988	0.728	0.858	0.0220	0.096	90.812	2.221
	RGB-NIR		0.990	0.753	0.872	0.0276	0.102	90.814	2.221	14.915
	WeedMap	RGB	0.985	0.526	0.756	0.0137	0.121	90.812	2.221	10.464
		RGB-NIR	0.985	0.538	0.762	0.0138	0.126	90.814	2.221	10.487
		RGB-NIR-RE	0.986	0.543	0.764	0.0140	0.129	90.816	2.221	10.511
	4	WeedBananaCOD	RGB	0.990	0.729	0.859	0.0214	0.094	90.583	1.991
RGB-NIR			0.991	0.740	0.865	0.0258	0.097	90.585	1.991	14.780
WeedMap		RGB	0.985	0.513	0.749	0.0127	0.118	90.583	1.991	10.369
		RGB-NIR	0.985	0.527	0.756	0.0127	0.123	90.585	1.991	10.393
		RGB-NIR-RE	0.985	0.530	0.758	0.0129	0.124	90.587	1.991	10.416
5		WeedBananaCOD	RGB	0.989	0.688	0.838	0.0214	0.090	90.449	1.857
	RGB-NIR		0.989	0.702	0.846	0.0248	0.095	90.451	1.857	14.725
	WeedMap	RGB	0.985	0.517	0.751	0.0125	0.114	90.449	1.857	10.330
		RGB-NIR	0.985	0.525	0.755	0.0123	0.125	90.451	1.857	10.354
		RGB-NIR-RE	0.986	0.530	0.758	0.0128	0.124	90.453	1.857	10.377

The ablation study on the kernel size (Table 4) of the DWConvs in the FCB shows that a 3×3 configuration achieves the best performance. Although larger kernels (5×5 and 7×7) expand the receptive field and capture broader context, this becomes counterproductive within the FCB block. Since the backbone (ConvNeXt) already extracts large scale contextual information (7×7 kernels), using larger kernels in the FCB appears to introduce redundancy that degrades local detail sharpness. Additionally, increasing the kernel size leads to higher latency, training time, and GFLOPs without improving performance.

Table 4. Ablation of the depthwise kernel size in the FCB block.

Kernel size	Dataset	Modality	IoU _{BC} ↑	IoU _w ↑	mIoU ↑	Inference time (s)	Training time (h)	Total params. (M)	Trainable params. (M)	GFLOPs
1	WeedBananaCOD	RGB	0.989	0.696	0.842	0.0225	0.096	91.269	2.677	15.141
		RGB-NIR	0.988	0.677	0.833	0.0296	0.103	91.271	2.677	15.174
	WeedMap	RGB	0.986	0.535	0.760	0.0130	0.123	91.269	2.677	10.646
		RGB-NIR	0.985	0.533	0.759	0.0137	0.135	91.271	2.677	10.669
		RGB-NIR-RE	0.986	0.537	0.761	0.0139	0.140	91.273	2.677	10.693
	3	WeedBananaCOD	RGB	0.991	0.733	0.862	0.0227	0.099	91.277	2.685
RGB-NIR			0.991	0.762	0.877	0.0298	0.105	91.279	2.685	15.190
WeedMap		RGB	0.985	0.534	0.760	0.0141	0.128	91.277	2.685	10.657
		RGB-NIR	0.986	0.545	0.766	0.0145	0.134	91.279	2.685	10.680
		RGB-NIR-RE	0.987	0.547	0.767	0.0147	0.142	91.281	2.685	10.704
5		WeedBananaCOD	RGB	0.990	0.724	0.857	0.0248	0.103	91.292	2.700
	RGB-NIR		0.990	0.753	0.872	0.0300	0.107	91.294	2.700	15.221
	WeedMap	RGB	0.986	0.532	0.759	0.0168	0.132	91.292	2.700	10.679
		RGB-NIR	0.986	0.540	0.763	0.0169	0.141	91.294	2.700	10.703
		RGB-NIR-RE	0.986	0.543	0.765	0.0173	0.147	91.299	2.700	10.726
	7	WeedBananaCOD	RGB	0.988	0.682	0.835	0.0253	0.105	91.315	2.724
RGB-NIR			0.991	0.736	0.863	0.0309	0.109	91.317	2.724	15.269
WeedMap		RGB	0.985	0.527	0.756	0.0176	0.132	91.315	2.724	10.712
		RGB-NIR	0.986	0.535	0.761	0.0178	0.144	91.317	2.724	10.736
		RGB-NIR-RE	0.986	0.533	0.760	0.0174	0.147	91.319	2.724	10.759

The ablation study on the FPN feature dimension (Table 5) shows that a dimension of 128 represents the optimal balance between performance and efficiency. A non-linear be-

havior is observed, where performance drops when increasing to 160, followed by a slight recovery at 192 without reaching the previous peak. This phenomenon suggests that increasing the dimensionality beyond 128 introduces structural redundancy that initially hinders convergence and dilutes encoder signals. Although a capacity of 192 allows the model to reorganize part of this information, the exponential increase in GFLOPs (from 15.1 to 28.4 for WeedBananaCOD) and latency confirms that higher dimensions saturate the decoder without providing meaningful improvements in data representational quality.

Table 5. Ablation study of the FPN feature dimension.

Feature dim.	Dataset	Modality	IoU _{BC} ↑	IoU _w ↑	mIoU ↑	Inference time (s)	Training time (h)	Total params. (M)	Trainable params. (M)	GFLOPs
96	WeedBananaCOD	RGB	0.990	0.717	0.853	0.0222	0.093	90.763	2.172	10.448
		RGB-NIR	0.991	0.739	0.865	0.0292	0.095	90.765	2.172	10.482
	WeedMap	RGB	0.986	0.524	0.755	0.0130	0.126	90.763	2.172	7.346
		RGB-NIR	0.986	0.530	0.758	0.0132	0.133	90.765	2.172	7.370
		RGB-NIR-RE	0.984	0.537	0.761	0.0135	0.142	90.767	2.172	7.393
	128	WeedBananaCOD	RGB	0.991	0.733	0.862	0.0227	0.099	91.277	2.685
RGB-NIR			0.991	0.762	0.877	0.0298	0.105	91.279	2.685	15.190
WeedMap		RGB	0.985	0.534	0.760	0.0141	0.128	91.277	2.685	10.657
		RGB-NIR	0.986	0.545	0.766	0.0145	0.134	91.279	2.685	10.680
		RGB-NIR-RE	0.987	0.547	0.767	0.0147	0.142	91.281	2.685	10.704
160		WeedBananaCOD	RGB	0.989	0.719	0.854	0.0252	0.105	91.919	3.328
	RGB-NIR		0.990	0.748	0.869	0.0308	0.108	91.921	3.328	21.205
	WeedMap	RGB	0.986	0.526	0.756	0.0170	0.132	91.919	3.328	14.886
		RGB-NIR	0.983	0.535	0.759	0.0171	0.143	91.920	3.328	14.910
		RGB-NIR-RE	0.986	0.541	0.764	0.0177	0.151	91.923	3.328	14.934
	192	WeedBananaCOD	RGB	0.990	0.731	0.861	0.0260	0.107	92.691	4.099
RGB-NIR			0.991	0.750	0.871	0.0316	0.110	92.693	4.099	28.528
WeedMap		RGB	0.983	0.527	0.755	0.0170	0.131	92.691	4.099	20.035
		RGB-NIR	0.986	0.542	0.764	0.0173	0.147	92.693	4.099	20.059
		RGB-NIR-RE	0.985	0.545	0.765	0.0179	0.153	92.695	4.099	20.082

The ablation of refine depth in Table 6 shows that integrating two refinement blocks achieves the optimal balance between noise suppression in the fused FPN features and preservation of spatial detail. Exceeding this threshold leads to performance degradation. This is likely due to excessive smoothing blocks introducing an over-smoothing effect that blurs fine details, saturating the model’s capacity and leading to overfitting without improving representational quality, despite the increase in parameters and the associated rise in computational cost.

The ablation shown in Table 7 demonstrates that integrating the FCB block is the determining factor for achieving optimal performance. The results indicate that the w/FCB configuration achieves the highest mIoU across all datasets and spectral modalities, significantly outperforming both the baseline model (w/o FCB) and the alternative using CBAM. When the FCB is removed, a marked performance drop is observed, indicating that the frozen backbone alone lacks the necessary adaptation capacity for multispectral segmentation. In contrast, replacing the FCB with the CBAM attention block does not provide meaningful benefits; although CBAM presents fewer theoretical parameters and GFLOPs, this does not translate into real efficiency, resulting in noticeably higher training and inference times. This behavior confirms that CBAM operations are more costly in practice, while the FCB achieves the best balance between robustness, lower latency, and prediction accuracy.

The performance of all FCBNet variants is presented in

Table 6. Ablation of the decoder refinement depth.

Refine depth	Dataset	Modality	IoU _{BC} ↑	IoU _W ↑	mIoU ↑	Inference time (s)	Training time (h)	Total params. (M)	Trainable params. (M)	GFLOPS
0	WeedBananaCOD	RGB	0.990	0.716	0.853	0.0219	0.093	90.981	2.390	10.312
		RGB-NIR	0.990	0.731	0.860	0.0226	0.094	90.983	2.390	10.346
	WeedMap	RGB	0.985	0.509	0.747	0.0140	0.131	90.981	2.390	7.251
		RGB-NIR	0.986	0.521	0.753	0.0144	0.135	90.983	2.390	7.274
		RGB-NIR-RE	0.986	0.530	0.758	0.0146	0.135	90.985	2.390	7.298
	WeedBananaCOD	RGB	0.990	0.713	0.852	0.0219	0.095	91.129	2.537	12.734
RGB-NIR		0.991	0.741	0.866	0.0229	0.097	91.131	2.537	12.768	
1	WeedMap	RGB	0.984	0.520	0.752	0.0145	0.133	91.129	2.537	8.954
		RGB-NIR	0.985	0.527	0.756	0.0146	0.133	91.131	2.537	8.977
		RGB-NIR-RE	0.986	0.539	0.762	0.0147	0.139	91.133	2.537	9.001
WeedBananaCOD	RGB	0.991	0.733	0.862	0.0227	0.099	91.277	2.685	15.156	
	RGB-NIR	0.991	0.762	0.877	0.0298	0.105	91.279	2.685	15.190	
2	WeedMap	RGB	0.985	0.534	0.760	0.0141	0.128	91.277	2.685	10.657
		RGB-NIR	0.986	0.545	0.766	0.0145	0.134	91.279	2.685	10.680
		RGB-NIR-RE	0.987	0.547	0.767	0.0147	0.142	91.281	2.685	10.704
WeedBananaCOD	RGB	0.990	0.725	0.857	0.0251	0.105	91.424	2.833	17.579	
	RGB-NIR	0.991	0.755	0.872	0.0278	0.107	91.426	2.833	17.612	
3	WeedMap	RGB	0.984	0.504	0.744	0.0150	0.131	91.424	2.833	12.360
		RGB-NIR	0.986	0.540	0.763	0.0154	0.141	91.426	2.833	12.383
		RGB-NIR-RE	0.986	0.543	0.764	0.0157	0.145	91.428	2.833	12.407
WeedBananaCOD	RGB	0.989	0.693	0.841	0.0249	0.106	91.572	2.981	20.001	
	RGB-NIR	0.990	0.737	0.864	0.0263	0.107	91.574	2.981	20.034	
4	WeedMap	RGB	0.985	0.519	0.752	0.0153	0.138	91.572	2.981	14.063
		RGB-NIR	0.986	0.531	0.759	0.0153	0.142	91.574	2.981	14.087
		RGB-NIR-RE	0.987	0.536	0.762	0.0161	0.147	91.576	2.981	14.110
WeedBananaCOD	RGB	0.990	0.714	0.852	0.0268	0.108	91.720	3.128	22.423	
	RGB-NIR	0.990	0.719	0.855	0.0276	0.110	91.722	3.128	22.457	
5	WeedMap	RGB	0.986	0.527	0.756	0.0161	0.140	91.720	3.128	15.766
		RGB-NIR	0.981	0.529	0.759	0.0165	0.142	91.722	3.128	15.790
		RGB-NIR-RE	0.985	0.535	0.760	0.0167	0.146	91.724	3.128	15.813

Table 7. Comparison of the proposed FCB with other alternatives.

Component	Dataset	Modality	IoU _{BC} ↑	IoU _W ↑	mIoU ↑	Inference time (s)	Training time (h)	Total params. (M)	Trainable params. (M)	GFLOPS
	WeedBananaCOD	RGB	0.988	0.664	0.826	0.0223	0.093	89.871	1.280	14.053
		RGB-NIR	0.989	0.693	0.841	0.0250	0.094	89.874	1.280	14.087
w/o FCB	WeedMap	RGB	0.978	0.514	0.746	0.0131	0.121	89.871	1.280	9.881
		RGB-NIR	0.981	0.519	0.750	0.0134	0.125	89.874	1.280	9.905
		RGB-NIR-RE	0.982	0.521	0.752	0.0134	0.130	89.876	1.280	9.928
WeedBananaCOD	RGB	0.989	0.710	0.850	0.0382	0.140	90.048	1.457	14.056	
	RGB-NIR	0.988	0.693	0.840	0.0421	0.144	90.050	1.457	14.089	
w/CBAM	WeedMap	RGB	0.978	0.521	0.750	0.0282	0.188	90.048	1.457	9.883
		RGB-NIR	0.983	0.518	0.751	0.0286	0.194	90.050	1.457	9.906
		RGB-NIR-RE	0.985	0.523	0.754	0.0292	0.202	90.052	1.457	9.930
WeedBananaCOD	RGB	0.991	0.733	0.862	0.0227	0.099	91.277	2.685	15.156	
	RGB-NIR	0.991	0.762	0.877	0.0298	0.105	91.279	2.685	15.190	
w/FCB	WeedMap	RGB	0.985	0.534	0.760	0.0141	0.128	91.277	2.685	10.657
		RGB-NIR	0.986	0.545	0.766	0.0145	0.134	91.279	2.685	10.680
		RGB-NIR-RE	0.987	0.547	0.767	0.0147	0.142	91.281	2.685	10.704

Table 8. The results show a consistent improvement in performance as the encoder scale increases, across both RGB and multispectral configurations in both datasets. In terms of efficiency, the expected increase in latency and training time is observed when scaling the architecture; however, the number of trainable parameters remains notably low due to the freezing strategy. In the Tiny variant, the number of trainable parameters is reduced from 30.6M to only 2.01M, representing a 93.4% reduction, while the Large variant achieves a massive reduction of 97.7%. This allows even the most complex model to be trained in approximately 0.2 hours, validating FCBNet as a flexible model whose structural efficiency enables the deployment of both lightweight and robust models under limited computational resources.

Finally, Table 9 presents the comparison between the proposed architecture and several state of the art methods. The results show that FCBNet-large achieves the highest performance across both datasets and all spectral modalities, suggesting a superior ability to adapt and effectively leverage information from multiple channels. It is also notable that, in the WeedMap dataset, all evaluated models exhibit a lower performance ceiling compared to WeedBananaCOD; however, FCBNet consistently outperforms

Table 8. Performance comparison of FCBNet across different ConvNeXt encoders.

Encoder	Dataset	Modality	IoU _{BC} ↑	IoU _W ↑	mIoU ↑	Inference time (s)	Training time (h)	Total params. (M)	Trainable params. (M)	GFLOPS
ConvNeXt-tiny	WeedBananaCOD	RGB	0.990	0.717	0.853	0.0139	0.060	0.060	2.015	13.151
		RGB-NIR	0.991	0.740	0.865	0.0149	0.062	0.065	2.015	13.176
	WeedMap	RGB	0.985	0.537	0.761	0.0095	0.083	0.064	2.015	9.247
		RGB-NIR	0.986	0.540	0.763	0.0103	0.091	0.065	2.015	9.264
		RGB-NIR-RE	0.986	0.543	0.764	0.0107	0.098	0.067	2.015	9.282
	WeedBananaCOD	RGB	0.987	0.658	0.822	0.0178	0.075	0.060	2.015	13.540
RGB-NIR		0.989	0.703	0.846	0.0200	0.080	0.065	2.015	13.565	
ConvNeXt-small	WeedMap	RGB	0.985	0.540	0.762	0.0132	0.107	0.107	2.015	9.520
		RGB-NIR	0.986	0.544	0.765	0.0144	0.113	0.113	2.015	9.538
ConvNeXt-base	WeedMap	RGB	0.985	0.534	0.760	0.0141	0.128	0.128	2.015	10.657
		RGB-NIR	0.986	0.545	0.766	0.0145	0.134	0.134	2.015	10.680
		RGB-NIR-RE	0.987	0.547	0.767	0.0147	0.142	0.142	2.015	10.704
WeedBananaCOD	RGB	0.991	0.733	0.862	0.0227	0.099	0.099	2.015	15.156	
	RGB-NIR	0.991	0.762	0.877	0.0298	0.105	0.105	2.015	15.190	
ConvNeXt-large	WeedMap	RGB	0.987	0.546	0.766	0.0252	0.201	0.201	4.555	13.714
		RGB-NIR	0.986	0.548	0.767	0.0251	0.211	0.211	4.555	13.749
		RGB-NIR-RE	0.987	0.551	0.769	0.0257	0.215	0.215	4.555	13.784

its competitors even under these data constraints.

On the other hand, although the FCBNet-tiny variant is slightly outperformed in mIoU by models such as DeepLabV3+ or SegFormer in certain scenarios, such as the WeedBananaCOD dataset, the performance gap is minimal compared to the substantial efficiency gains. While these models require training times exceeding 0.12 and 0.31 hours respectively and exhibit significantly higher GFLOPs, FCBNet-tiny achieves competitive performance with only 0.06 hours of training. Overall, these results validate the superiority of the proposed approach, establishing it as a highly efficient solution that drastically reduces computational requirements without compromising accuracy compared to the other heavy methods in the literature.

To complement the quantitative analysis, Figs. 6a and 6b present a visual comparison of inference on the WeedBananaCOD and WeedMap datasets, respectively, using their full modalities. In WeedBananaCOD, FCBNet achieves more precise instance delineation and a significant reduction in false detections (rows b and d), producing results that more closely match the ground truth compared to the other models. In WeedMap, despite the sparse distribution and small size of weed instances, the proposed architecture also demonstrates a greater ability to identify small objects with a lower error rate. In both cases, the qualitative results confirm that the FCBNet correction mechanism better preserves fine details and improves the spatial coherence of the segmentation.

5. Limitations and Future work

Despite the evaluation across multiple datasets, spectral modalities, and ablation tests, we acknowledge limitations that define future research directions. First, the evaluation can be extended to other datasets containing additional scenarios, spectral bands, and classes (crops or different weed species), as this study focused on binary segmentation.

Furthermore, evaluating FCBNet on specialized hardware and embedded systems, such as Raspberry Pi or UAV

Table 9. FCBNet compared to other approaches from the literature. We have selected the best and lightest FCBNet model for comparison.

Encoder	Dataset	Modality	IoU _{BG} ↑	IoU _W ↑	mIoU ↑	Inference time (s)	Training time (h)	Total params. (M)	Trainable params. (M)	GFLOPS
FCBNet-tiny	WeedBananaCOD	RGB	0.990	0.717	0.853	0.0139	0.060	30.604	2.015	13.151
		RGB-NIR	0.991	0.740	0.865	0.0149	0.062	30.605	2.015	13.176
	WeedMap	RGB	0.985	0.537	0.761	0.0095	0.083	30.604	2.015	9.247
		RGB-NIR	0.986	0.540	0.763	0.0103	0.091	30.605	2.015	9.264
		RGB-NIR-RE	0.986	0.543	0.764	0.0107	0.098	30.607	2.015	9.282
			0.991	0.746	0.868	0.0360	0.169	202.322	4.555	19.504
FCBNet-large	WeedBananaCOD	RGB-NIR	0.992	0.771	0.881	0.0381	0.171	202.325	4.555	19.554
		0.987	0.546	0.766	0.0252	0.201	202.322	4.555	13.714	
	WeedMap	RGB-NIR	0.986	0.548	0.767	0.0251	0.211	202.325	4.555	13.749
		RGB-NIR-RE	0.987	0.551	0.769	0.0257	0.215	202.329	4.555	13.784
			0.984	0.596	0.790	0.0223	0.089	12.721	12.721	12.731
		WeedBananaCOD	RGB-NIR	0.986	0.625	0.805	0.0225	0.093	12.723	12.723
WeedSense [33]	RGB		0.979	0.471	0.725	0.0115	0.138	12.721	12.721	8.952
	WeedMap	RGB-NIR	0.984	0.515	0.749	0.0190	0.151	12.723	12.723	8.985
		RGB-NIR-RE	0.984	0.519	0.752	0.0196	0.166	12.724	12.724	9.018
	DeepLabV3+ [3]	WeedBananaCOD	RGB	0.988	0.721	0.855	0.0270	0.123	26.678	26.678
RGB-NIR			0.991	0.725	0.858	0.0390	0.125	26.681	26.681	36.968
WeedMap		RGB	0.983	0.509	0.746	0.0190	0.161	26.678	26.678	25.849
		RGB-NIR	0.984	0.515	0.749	0.0190	0.170	26.681	26.681	25.993
		RGB-NIR-RE	0.986	0.534	0.760	0.0200	0.189	26.684	26.684	26.137
			0.990	0.715	0.851	0.0243	0.097	32.521	32.521	42.771
U-Net [29]	WeedBananaCOD	RGB-NIR	0.990	0.720	0.855	0.0257	0.100	32.524	32.524	42.976
		0.975	0.427	0.701	0.0109	0.119	32.521	32.521	30.073	
	WeedMap	RGB-NIR	0.981	0.508	0.745	0.0112	0.126	32.524	32.524	30.218
		RGB-NIR-RE	0.986	0.550	0.768	0.0117	0.131	32.528	32.528	30.362
			0.989	0.695	0.842	0.0203	0.310	84.595	84.595	49.733
		WeedBananaCOD	RGB-NIR	0.990	0.738	0.864	0.0295	0.312	84.598	84.598
WeedMap	RGB		0.986	0.506	0.746	0.0177	0.420	84.595	84.595	34.116
	RGB-NIR	0.985	0.532	0.758	0.0180	0.421	84.598	84.598	34.153	
	RGB-NIR-RE	0.985	0.535	0.760	0.0189	0.421	84.601	84.601	34.189	
		0.986	0.641	0.813	0.0231	0.170	34.444	34.444	44.745	
SK-U-Net [25]	WeedBananaCOD	RGB-NIR	0.990	0.705	0.847	0.0238	0.170	34.447	34.447	44.950
		0.983	0.532	0.758	0.0140	0.160	34.444	34.444	31.461	
	WeedMap	RGB-NIR	0.982	0.539	0.761	0.0164	0.170	34.447	34.447	31.606
		RGB-NIR-RE	0.984	0.539	0.762	0.0140	0.178	34.450	34.450	31.751

platforms, would provide valuable complementary validation of its behaviour under real deployment conditions.

Finally, exploring structural modifications, including the use of dual encoders for multispectral processing or the integration of alternative decoder designs, represents a natural research direction derived from this work.

6. Conclusions

We introduce FCBNet, an efficient architecture for weed detection. It employs a frozen ConvNeXt backbone integrated with the proposed FCB block, which combines efficient convolutions to refine feature representations at minimal computational cost, along with a lightweight FPN decoder. Extensive evaluations on the WeedBananaCOD and WeedMap datasets demonstrate that FCBNet outperforms established models such as U-Net, SK-U-Net, SegFormer, and WeedSense in both mIoU and operational efficiency. Specifically, the freezing strategy enables a reduction of trainable parameters >93%, achieving training times of only 0.06 to 0.2 hours without compromising performance.

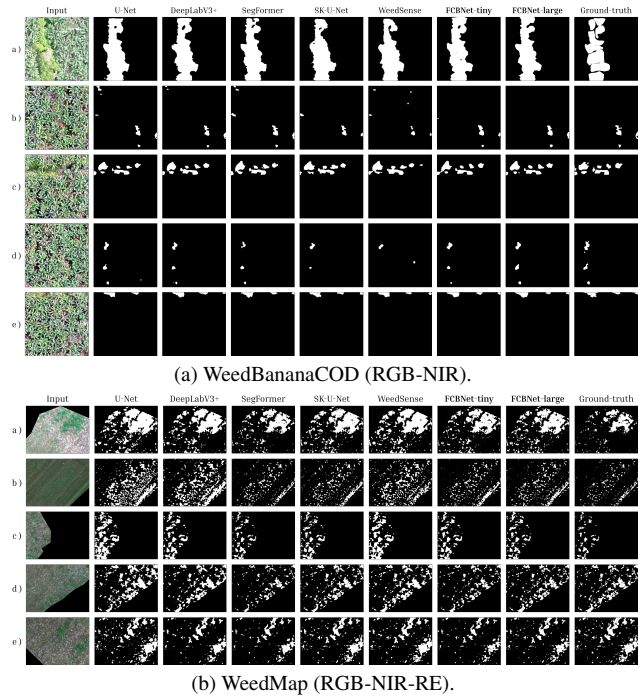


Figure 6. Qualitative comparison between FCBNet and other models from the state-of-the-art. Zoom in for better visualization.

References

- [1] Dong Chen, Yuzhen Lu, Zhaojian Li, and Sierra Young. Performance evaluation of deep transfer learning on multi-class identification of common weed species in cotton production systems. *Comput. Electron. Agric.*, 198:107091, 2022. 1
- [2] Dong Chen, Xinda Qi, Yu Zheng, Yuzhen Lu, Yanbo Huang, and Zhaojian Li. Synthetic data augmentation by diffusion probabilistic models to enhance weed recognition. *Comput. Electron. Agric.*, 216:108517, 2024. 1
- [3] Liang-Chieh Chen, Yukun Zhu, George Papandreou, Florian Schroff, and Hartwig Adam. Encoder-decoder with atrous separable convolution for semantic image segmentation. In *ECCV*, 2018. 5, 8
- [4] Pengguang Chen, Shu Liu, Hengshuang Zhao, and Jiaya Jia. Distilling knowledge via knowledge review. In *CVPR*, 2021. 1
- [5] Fengying Dang, Dong Chen, Yuzhen Lu, and Zhaojian Li. Yoloweeds: A novel benchmark of yolo object detectors for multi-class weed detection in cotton production systems. *Comput. Electron. Agric.*, 205:107655, 2023. 1
- [6] Boyang Deng, Yuzhen Lu, and Jiajun Xu. Weed database development: An updated survey of public weed datasets and cross-season weed detection adaptation. *Ecol. Inform.*, 81:102546, 2024. 1
- [7] Mohammed El Hafyani, Amine Saddik, Mohammed Hsaisoune, Adnane Labbaci, Abdellaali Tairi, Fatima Abdelfadel, and Lhoussaine Bouchaou. Weeds detection in a citrus orchard using multispectral uav data and machine learning algorithms: A case study from souss-massa basin, morocco. *Remote Sens. Environ.*, 38:101553, 2025. 1
- [8] Jianping Gou, B. Yu, S. Maybank, and D. Tao. Knowledge distillation: A survey. *Int. J. Comput. Vis.*, 129:1789–1819, 2021. 1
- [9] Zhiming Guo, Yi Xue, Chuan Wang, Yuhang Geng, Ruoyu Lu, Hailong Li, Deng Sun, Zhaoxia Lou, Tianbao Chen, Jianzhe Shi, and Longzhe Quan. Efficient weed segmentation in maize fields: A semi-supervised approach for precision weed management with reduced annotation overhead. *Comput. Electron. Agric.*, 229:109707, 2025. 2
- [10] Sanjay Kumar Gupta, Shivam Kumar Yadav, Sanjay Kumar Soni, Udai Shanker, and Pradeep Kumar Singh. Multiclass weed identification using semantic segmentation: An automated approach for precision agriculture. *Ecol. Inform.*, 78:102366, 2023. 2
- [11] Jessica B. Hopson, Anthime Flaus, Colm J. McGinnity, Radhouene Neji, Andrew J. Reader, and Alexander Hammers. Deep convolutional backbone comparison for automated pet image quality assessment. *IEEE TRPMS*, 8(8):893–901, 2024. 1
- [12] Md. Jawadul Karim, Md. Nahiduzzaman, Mominul Ahsan, and Julfikar Haider. Development of an early detection and automatic targeting system for cotton weeds using an improved lightweight yolov8 architecture on an edge device. *Knowl.-Based Syst.*, 300:112204, 2024. 1
- [13] Davood Karimi, Simon K. Warfield, and Ali Gholipour. Transfer learning in medical image segmentation: New insights from analysis of the dynamics of model parameters and learned representations. *Artif. Intell. Med.*, 116:102078, 2021. 1
- [14] Ashish Kaushal, Osama Almurshed, Areej Alabbas, Nitin Auluck, and Omer Rana. An edge-cloud infrastructure for weed detection in precision agriculture. In *IEEE IDASC/PiCom/CBDCom/CyberSciTech*, 2023. 1
- [15] Juan Liao, Minhui Chen, Kai Zhang, Huiyu Zhou, Yu Zou, Wei Xiong, Shun Zhang, Fuming Kuang, and Dequan Zhu. Sc-net: A new strip convolutional network model for rice seedling and weed segmentation in paddy field. *Comput. Electron. Agric.*, 220:108862, 2024. 1, 2
- [16] Tsung-Yi Lin, Piotr Dollar, Ross Girshick, Kaiming He, Bharath Hariharan, and Serge Belongie. Feature pyramid networks for object detection. In *CVPR*, 2017. 2
- [17] Zhuang Liu, Hanzi Mao, Chao-Yuan Wu, Christoph Feichtenhofer, Trevor Darrell, and Saining Xie. A convnet for the 2020s. In *CVPR*, 2022. 2
- [18] Rajesh U. Modi, Mrunalini Kancheti, A. Subeesh, Chandramani Raj, Akhilesh K. Singh, Narendra S. Chandel, Ashish S. Dhimate, Mrityunjai K. Singh, and Shweta Singh. An automated weed identification framework for sugarcane crop: A deep learning approach. *Crop Prot.*, 173:106360, 2023. 1
- [19] Nenavath Srinivas Naik and Harshit Kumar Chaubey. Weed detection and classification in sesame crops using region-based convolution neural networks. *Neural Comput. Appl.*, 36:18961–18977, 2024. 1
- [20] Shuteng Niu, Yongxin Liu, Jian Wang, and Houbing Song. A decade survey of transfer learning (2010–2020). *IEEE TAI*, 1(2):151–166, 2020. 1
- [21] Deepthi G Pai, Radhika Kamath, and Mamatha Balachandra. Deep learning techniques for weed detection in agricultural environments: A comprehensive review. *IEEE Access*, 12:113193–113214, 2024. 1
- [22] Hongxing Peng, Zihe Li, Zhiyan Zhou, and Yuanyuan Shao. Weed detection in paddy field using an improved retinanet network. *Comput. Electron. Agric.*, 199:107179, 2022. 1
- [23] Rekha Raja, Wen-Hao Su, David C. Slaughter, and Steven A. Fennimore. Real-time precision crop identification in high weed-density environments for robotic weed control using spectral fluorescence imaging in celery. *Comput. Electron. Agric.*, 231:110022, 2025. 1
- [24] Leo Thomas Ramos and Angel D. Sappa. Multispectral semantic segmentation for land cover classification: An overview. *IEEE JSTARS*, 17:14295–14336, 2024. 1
- [25] Leo Thomas Ramos and Angel D. Sappa. Leveraging u-net and selective feature extraction for land cover classification using remote sensing imagery. *Sci. Rep.*, 15(1):784, 2025. 5, 8
- [26] Leo Thomas Ramos and Angel D. Sappa. Multi-encoder convnext network with smooth attentional feature fusion for multispectral semantic segmentation. *arXiv preprint arXiv:2602.10137*, 2026. 3
- [27] Najmeh Razfar, Julian True, Rodina Bassiouny, Vishaal Venkatesh, and Rasha Kashef. Weed detection in soybean crops using custom lightweight deep learning models. *J. Agric. Food Res.*, 8:100308, 2022. 1, 2

- [28] Mobeen Ur Rehman, Hassan Eesaar, Zeeshan Abbas, Lakmal Seneviratne, Irfan Hussain, and Kil To Chong. Advanced drone-based weed detection using feature-enriched deep learning approach. *Knowl.-Based Syst.*, 305:112655, 2024. 1
- [29] Olaf Ronneberger, Philipp Fischer, and Thomas Brox. U-net: Convolutional networks for biomedical image segmentation. In *MICCAI*, 2015. 5, 8
- [30] Inkyu Sa, Marija Popović, Raghav Khanna, Zetao Chen, Philipp Lottes, Frank Liebisch, Juan Nieto, Cyril Stachniss, Achim Walter, and Roland Siegwart. Weedmap: A large-scale semantic weed mapping framework using aerial multispectral imaging and deep neural network for precision farming. *Remote Sens.*, 10(9), 2018. 5
- [31] Halil Mertkan Sahin, Tajul Miftahushudur, Bruce Grieve, and Hujun Yin. Segmentation of weeds and crops using multispectral imaging and crf-enhanced u-net. *Comput. Electron. Agric.*, 211:107956, 2023. 1, 2
- [32] Bishwa B. Sapkota, Sorin Popescu, Nithya Rajan, Ramon G. Leon, Chris Reberg-Horton, Steven Mirsky, and Muthukumar V. Bagavathiannan. Use of synthetic images for training a deep learning model for weed detection and biomass estimation in cotton. *Sci. Rep.*, 12(1):19580, 2022. 1
- [33] Toqi Tahamid Sarker, Khaled R Ahmed, Taminul Islam, Cristiana Bernardi Rankrape, and Karla Gage. Weedsense: Multi-task learning for weed segmentation, height estimation, and growth stage classification. In *ICCVW*, 2025. 5, 8
- [34] Akhilesh Sharma, Vipin Kumar, and Louis Longchamps. Comparative performance of yolov8, yolov9, yolov10, yolov11 and faster r-cnn models for detection of multiple weed species. *Smart Agric. Technol.*, 9:100648, 2024. 1
- [35] Vyomika Singh, Dharmendra Singh, and Harish Kumar. Efficient application of deep neural networks for identifying small and multiple weed patches using drone images. *IEEE Access*, 12:71982–71996, 2024. 1, 2
- [36] Jinya Su, Dewei Yi, Matthew Coombes, Cunjia Liu, Xiaojun Zhai, Klaus McDonald-Maier, and Wen-Hua Chen. Spectral analysis and mapping of blackgrass weed by leveraging machine learning and uav multispectral imagery. *Comput. Electron. Agric.*, 192:106621, 2022. 1
- [37] Boyi Tang, Jingping Zhou, Chunjiang Zhao, Yuchun Pan, Yao Lu, Chang Liu, Kai Ma, Xuguang Sun, Ruifang Zhang, and Xiaohe Gu. Using uav-based multispectral images and cgs-yolo algorithm to distinguish maize seeding from weed. *Artif. Intell. Agric.*, 15(2):162–181, 2025. 1, 2
- [38] Henry O. Velesaca, Andrea Mero, Hector Villegas, and Angel D. Sappa. Unveiling the hidden: Early detection of invasive vegetation in crops with uav multispectral imaging. *Smart Agric. Technol.*, page 101875, 2026. 5
- [39] Lin Wang and Kuk-Jin Yoon. Knowledge distillation and student-teacher learning for visual intelligence: A review and new outlooks. *IEEE TPAMI*, 44(6):3048–3068, 2022. 1
- [40] Paul Wimmer, Jens Mehnert, and Alexandru Paul Condurache. Dimensionality reduced training by pruning and freezing parts of a deep neural network: a survey. *Artif. Intell. Rev.*, 56(12):14257–14295, 2023. 1
- [41] Enze Xie, Wenhai Wang, Zhiding Yu, Anima Anandkumar, Jose M. Alvarez, and Ping Luo. Segformer: simple and efficient design for semantic segmentation with transformers. In *NeurIPS*, 2021. 5, 8
- [42] Ke Xu, Peter Yuen, Qi Xie, Yan Zhu, Weixing Cao, and Jun Ni. Weedsnet: a dual attention network with rgb-d image for weed detection in natural wheat field. *Precis. Agric.*, 25(1):460–485, 2023. 1
- [43] Hua Zhang, Zhengang Jiang, Guoxun Zheng, and Xuekun Yao. Semantic segmentation of high-resolution remote sensing images with improved u-net based on transfer learning. *Int. J. Comput. Intell. Syst.*, 16(181):1–11, 2023. 1
- [44] Miao Zhang, Harvineet Singh, Lazarus Chok, and Rumi Chunara. Segmenting across places: The need for fair transfer learning with satellite imagery. In *CVPRW*, 2022. 1
- [45] Fuzhen Zhuang, Zhiyuan Qi, Keyu Duan, Dongbo Xi, Yongchun Zhu, Hengshu Zhu, Hui Xiong, and Qing He. A comprehensive survey on transfer learning. *Proc. IEEE*, 109(1):43–76, 2021. 1
- [46] Riaan Zoetmulder, Efstratios Gavves, Matthan Caan, and Henk Marquering. Domain- and task-specific transfer learning for medical segmentation tasks. *Comput. Methods Programs Biomed.*, 214:106539, 2022. 1
- [47] Kunlin Zou, Xin Chen, Yonglin Wang, Chunlong Zhang, and Fan Zhang. A modified u-net with a specific data argumentation method for semantic segmentation of weed images in the field. *Comput. Electron. Agric.*, 187:106242, 2021. 2